Journal of Materials Chemistry C

ROYAL SOCIETY OF CHEMISTRY

COMMUNICATION

View Article Online
View Journal | View Issue

Cite this: J. Mater. Chem. C, 2025, 13, 22973

Received 16th September 2025,
Accepted 7th November 2025

DOI: 10.1039/d5tc03451e

rsc.li/materials-c

Metal organic frameworks as molecular encapsulants to prevent efficiency losses in perovskite solar cells

Lorenzo Pancini,[a] Francesco Toniolo,[a] Diego Mirani,[b] Filippo Doria *[a] and Giulia Grancini *[a]

Perovskite solar cells (PSCs) exhibit exceptional power conversion efficiencies; however, their commercial deployment remains hindered by pronounced instability under environmental stressors such as moisture, oxygen, elevated temperatures, and ultraviolet (UV) radiation. In this work, we present the design and integration of mixed-matrix thermoplastic polyurethane (TPU) encapsulant films embedded with zeolitic imidazolate framework-8 (ZIF-8) and its fluorinated-silane–functionalized analogue (F-ZIF8). These films serve as intermediate barrier layers in the glass–glass encapsulation architecture of p–i–n structured PSCs employing a triple-cation perovskite composition ($Cs_{0.03}MA_{0.07}FA_{0.9}PbI_3$). The incorporation of MOF nanofillers imparts a tortuous diffusion pathway that significantly impedes moisture ingress, while maintaining a low lamination temperature (~110 °C) compatible with the thermal sensitivity of the perovskite absorber layer. Under accelerated humidity aging conditions (relative humidity >85%, 25 °C), devices encapsulated with TPU/ZIF8 and TPU/F-ZIF8 retained 84% and 81%, respectively, of their initial power conversion efficiency (PCE) after 70 days. In contrast, devices encapsulated with pristine TPU exhibited a markedly shorter T_{80} lifetime of only 25 days. These findings highlight the potential of MOF-based mixed-matrix TPU films as high-performance encapsulants, capable of enhancing the operational durability of PSCs under harsh environmental conditions. This approach represents a viable strategy toward the development of commercially relevant perovskite photovoltaic technologies with prolonged service lifetimes.

Introduction

The perovskite active material in PSCs is highly susceptible to degradation due to humidity,[1] oxygen,[2] light,[3] and temperature,[4] which can reduce the durability and performance of the devices.

To overcome these stability challenges and render PSCs commercially viable, advanced encapsulation strategies have been pursued. An ideal encapsulant must combine high optical transparency across the perovskite absorption spectrum,[5] cost-effectiveness,[6] and compatibility with large-scale manufacturing,[7] while also providing excellent barriers to oxygen and moisture ingress (*i.e.*, low WVTR and OTR[8]), as well as long-term mechanical, thermal, and chemical stability sufficient to sustain device performance for more than two decades. Encapsulation approaches for PSCs generally fall into three main categories: thin-film encapsulation (TFE),[5] polymer-based encapsulation,[9] and glass–glass encapsulation.[7] In TFE, alternating organic layers (*e.g.*, PMMA,[10] TPU,[11] PDMS,[12] or pV_3D_3[13]) and inorganic coatings (such as Al_2O_3,[14] SiO_2,[15] or SnO_x[16]) are deposited directly onto the cell. While this method can achieve ultralow WVTR values ($<10^{-5}$ g m^{-2} d^{-1})[17] with minimal film thickness, it relies on vacuum-based processes (sputtering, PECVD, ALD) that are costly, potentially damaging to the perovskite layer, and difficult to scale up.[9] In contrast, polymer-based encapsulation is inherently compatible with roll-to-roll processing[8] and benefits from readily available, inexpensive materials; however, it typically requires higher curing temperatures and exhibits inferior barrier performance (higher WVTR and OTR) relative to TFE.[9] Glass–glass encapsulation, by sealing the device between two glass substrates, offers a compelling alternative by combining robust protection with relatively low processing temperatures and straightforward scalability. Glass–glass encapsulation strikes an effective balance between cost and performance by vacuum-laminating the cell between two glass plates, sealing the edges with a perimeter adhesive, and filling the interior with a hot-melt polymer to limit gas ingress at the seal interface.[18] Optimal cap sealants must cure at low temperature[19] and adhere well to minimize moisture permeation. While EVA[20] and Surlyn[21]—common in silicon PV—degrade under aging (releasing acetic[22] and methacrylic acids[7]) and can delaminate contacts,[23] and POE[24]—chemically inert—it typically requires relatively high lamination temperatures (140–150 °C),[18,19,25] even though commercially available hot-melt

[a] Department of Chemistry & INSTM Università di Pavia, Via T. Taramelli 14, Pavia 27100, Italy. E-mail: giulia.grancini@unipv.it, filippo.doria@unipv.it
[b] Université Grenoble Alpes, CEA, CNRS, Grenoble-INP, IRIG-SyMMES, 17 avenue des Martyrs, Grenoble, 38000, France

polyolefins can be processed at temperatures below 100 °C.[26] In contrast, TPU[27] offers lower-temperature[28] processing (≈110 °C) yet suffers from relatively higher WVTR.

In this work, we evaluate TPU ST-6050 as a cap sealant for p–i–n $Cs_{0.03}MA_{0.07}FA_{0.9}PbI_3$ PSCs, enhancing its barrier properties by incorporating ZIF-8 and a perfluorodecyl-silane–modified ZIF-8 (F-ZIF8) into the polymer matrix. The MOF fillers, localized at the inner interface of cap sealant films, create a tortuous-pathway effect and, in the fluorinated variant, increase hydrophobicity, as evidenced by contact-angle and permeability measurements. Under 25 °C/95% RH aging, cells encapsulated with TPU/ZIF8 and TPU/F-ZIF8 maintain ≥80% of their initial PCE (T_{80}) beyond 70 days, compared to just 25 days for TPU alone—demonstrating a straightforward route to markedly improved PSC longevity.

Experimental section

Materials

Zinc nitrate hexahydrate ($Zn(NO_3)_2{\cdot}6H_2O$), 2-methylimidazole (Hmim), 1*H*,1*H*,2*H*,2*H*-perfluorodecyltriethoxysilane (PDTS), poly(vinylidene fluoride) (PVDF), ethanol (EtOH), methanol (MeOH), and *N*,*N*-dimethylacetamide (DMAc) were all purchased from Sigma-Aldrich.

ZIF8 synthesis

ZIF8 nanoparticles (NPs) were synthesized following the procedure reported by Steunou *et al.*[29] A solution of Hmim (6.50 g, 79.04 mmol) in 200 mL of MeOH was added to a solution of $Zn(NO_3)_2{\cdot}6H_2O$ (2.93 g, 9.87 mmol) in 200 mL of MeOH at room temperature under constant stirring. After 2 hours, the resulting milky solution was centrifuged at 9000 rpm for 45 minutes to recover the ZIF-8 NPs, which were then re-dispersed in 30 mL of absolute ethanol and centrifuged twice to ensure purity. The ZIF8 NPs were dried overnight at 100 °C, followed by ball milling for 10 minutes using 2 mm zirconia balls to produce ZIF8 powder with an average particle size of 4 μm.

Modified ZIF8 synthesis

Modified ZIF-8 was synthesized following the procedure reported by Zhang *et al.*,[30] as follows: 0.3 g of PVDF was dissolved in 9.7 g of DMAC under magnetic stirring for 2 hours. Next, 1.0 g of the homogeneous DMAC solution containing 3 wt% PVDF was combined with 8.8 g of ethanol under vigorous stirring for 30 minutes, followed by ultrasonication for 30 minutes. A 0.05 g portion of ZIF8 NPs was then dispersed in the suspension with additional ultrasonication. Finally, 0.1 g of PDTS was added to the mixture, and stirring continued for 12 hours, yielding a dispersion containing 0.3 wt% PVDF, 0.5 wt% ZIF8, and 1 wt% PDTS.

Mixed matrix membrane (MMM) TPU/ZIF8 and TPU/F-ZIF8

ZIF8 and modified ZIF8 dispersions in methanol and ethanol, respectively, were deposited onto the TPU surface by drop-casting to create a uniform superficial dispersion of the MOF across the TPU. The solvent was then evaporated using a hot plate, ensuring an homogeneous distribution of the filler.

Perovskite solar cells fabrication

For the fabrication of PSCs, indium tin oxide (ITO)-coated glass substrates were consecutively cleaned in deionized water, acetone and IPA by ultrasonicating for 15 min for each solvent. Substrates were dried with N_2 airflow and O_2 plasma treated for 10 min. MeO-2PACz was dissolved in ethanol with a concentration of 1 mM and 40 μL was spin-coated onto ITO/glass substrates and annealed at 100 °C for 10 min. The perovskite precursor solution (1.5 M) was prepared by dissolving PbI_2, FAI, MAI and MACl in a DMF/DMSO 4/1 solution. 30 μL of the final solution were deposited on the MeO-2PACz coated substrates and spin-coated with a two-step procedure: the first step proceeded at 5000 rpm for 27 s, while the last step was a speed reduction of 4 s. 120 μL of chlorobenzene, for an antisolvent procedure were poured on to the substrate after 21 seconds from the beginning of the second step. Subsequently, substrates were annealed at 100 °C for 30 minutes. To fabricate the ETL, PCBM was dissolved in chloroform to produce a 15 mg mL^{-1} solution. 20 μL of the solution were dynamically spin-coated onto the perovskite layer. To prevent the diffusion of the metal contact inside the perovskite 50 μL of 0.5 mg mL^{-1} solution (in isopropanol) of bathocuproine was deposited on PCBM. Finally, 80 nm of Ag was thermally evaporated on the device. The evaporation speed was adjusted to 0.01 nm s^{-1} for the first 5 nm, 0.02 nm s^{-1} from 5 to 15 nm, and 0.06 nm s^{-1} for the rest of the procedure. All solutions were prepared in an Ar-filled glovebox, while the deposition of each layer of the solar cell was performed in an N2-filled glovebox.

Encapsulation of perovskite solar cells

Encapsulation of perovskite solar cells (PSCs) was performed using a Radiant PV Equipment system *via* vacuum lamination. A total lamination time of 12 minutes was applied, with a vacuum ramp sequence consisting of −70 kPa for 120 seconds, −50 kPa for 60 seconds, and −30 kPa for 40 seconds, all at a constant temperature of 110 °C.

J–V Measurement

Current density–voltage (*J–V*) measurements were conducted under ambient conditions using simulated AM1.5 sunlight at an intensity of 100 mW cm^{-2} (Wavelabs-Sinus 70). The light intensity was calibrated with a Si reference cell. Measurements were carried out using a Keithley 2450 source-meter with backward and forward scans from 1.2 to −0.1 V at a scan rate of 100 mV s^{-1}. Each cell had an active area of 0.3 cm^2.

Contact angle measurements

The static water contact angle (CA) were evaluated using a OCA 30/DataPhysics.apparatus at ambient temperature.

XRD

X-ray diffraction patterns were obtained using a X'Pert Pro con X'Celerator Detector/Panalytical instrument Cu Kα beam (λ = 1.54 Å).

Moisture permeability measurements

Moisture permeability measurements have been conducted with EXTRA SOLUTION Permeh$_2$O instruments. The area of the sample is 50 cm^2, the measurements have been made at 23 °C, 85%RH condition. The measurements have a condition time of 4 hours. The measurements have been carried out with a flow of the gas carrier flow 11.84 ml min^{-1}.

Lag time

The lag time was determined graphically by plotting WVTR as a function of time. The linear stationary region of the curve was extrapolated, and the intercept of its tangent with the *x*-axis was taken as the lag time value.

SEM and EDX analysis

A Supra 55VP/Zeiss microscope + UltraMax 170 mm^2/Oxford Instruments have been used for the morphological characterization. The materials were supported on graphite biadhesives fixed on Al stubs and subsequently transferred in the SEM chamber. The measurements were performed under ultrahigh vacuum at a working distance of 8.5 mm and with an electron generation voltage of 10 kV.

Result and discussion

The ZIF8 used in this work was synthesized by combining $Zn(NO_3)_2$ and 2-methylimidazole in a solution-based method with methanol, following the procedure outlined by Steunou *et al.* This process yielded cubic ZIF8 crystals approximately 200 nm in size, as shown in SI1a. The modified F-ZIF8 was synthesized according to the procedure reported by Zhang and co-workers, where ZIF8 crystals were combined with polydodecafluoro-triethoxysilane (PDTS) and a fraction of PVDF as a compatibilizer, producing a homogeneous dispersion, as confirmed by SEM and EDX analyses (see SI1b).

The resulting MOF was dispersed in methanol (ZIF8) and ethanol (F-ZIF8) solution and drop-casting the solution onto the polymer surface allowed for the deposition of ZIF8 or modified F-ZIF8 at a concentration of 10% wt/wt, achieving a functionalized TPU layer (Fig. 1(b)). The polymer coated with ZIF8 and F-ZIF8 was then characterized for hydrophobicity through contact angle measurements to assess filler effectiveness. Conventional encapsulant polymers exhibit limited hydrophobicity. The contact angles (C.A.) of common encapsulant polymers range from 65° for polyimide (PI)[31] to 80° for polycarbonate (PC),[32] with polyethylene terephthalate (PET) and polyethylene naphthalate (PEN) showing intermediate values of 75° and 73°, respectively. Only the polyolefin elastomer (POE) reaches a C.A. of 88°, comparable with the functionalized TPU/ZIF-8 composite. As shown in Fig. 1(c), a clear trend is observed, with a contact angle (C.A.) of 69° for the unmodified TPU, rising from 87° for TPU/ZIF-8 to 130° for TPU/modified ZIF8, confirming the hydrophobic enhancement, particularly for the fluorinated modified ZIF8.

The surface functionalization of the polymer enables the use of the tortuous pathways effect. By incorporating ZIF8 and F-ZIF8, preferential pathways are created, decelerating the permeation of moisture molecules within the encapsulating polymer matrix. To exploit this effect, the MOF was first localized at the interface between the two TPU films used for encapsulation (Fig. 2(a)). The encapsulant must retain optical transparency in the wavelength range relevant to perovskite absorption to ensure efficient light harvesting; therefore, to minimize scattering and efficiency losses, the filler was positioned at the entire border of the TPU films. To further investigate the effect of the filler, permeability tests were conducted on both unmodified TPU and TPU functionalized with ZIF8 and F-ZIF8. In assessing encapsulant barrier performance, it is essential to consider not only permeability but also lag time. Permeability reflects the intrinsic ability of the encapsulant to act as a barrier, with lower values indicating better encapsulation properties. Additionally,

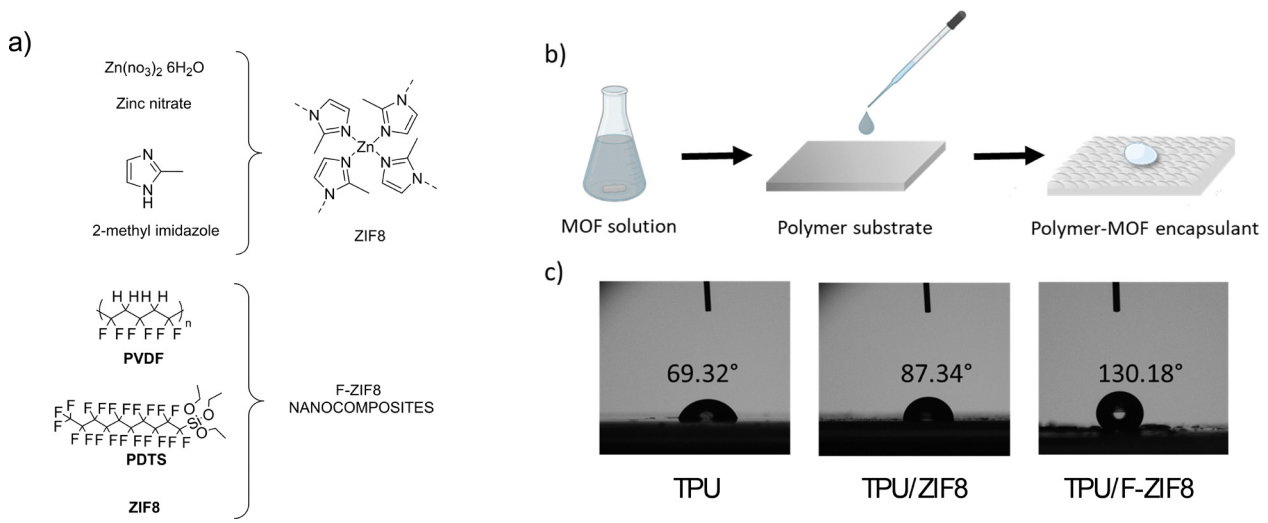

Fig. 1 Schematic representation of ZIF8 and modified F-ZIF8 materials (a); fabrication process of MOF-funcitonalized polymer (b); water contact angle measurements of TPU and TPU after MOF deposition (c).

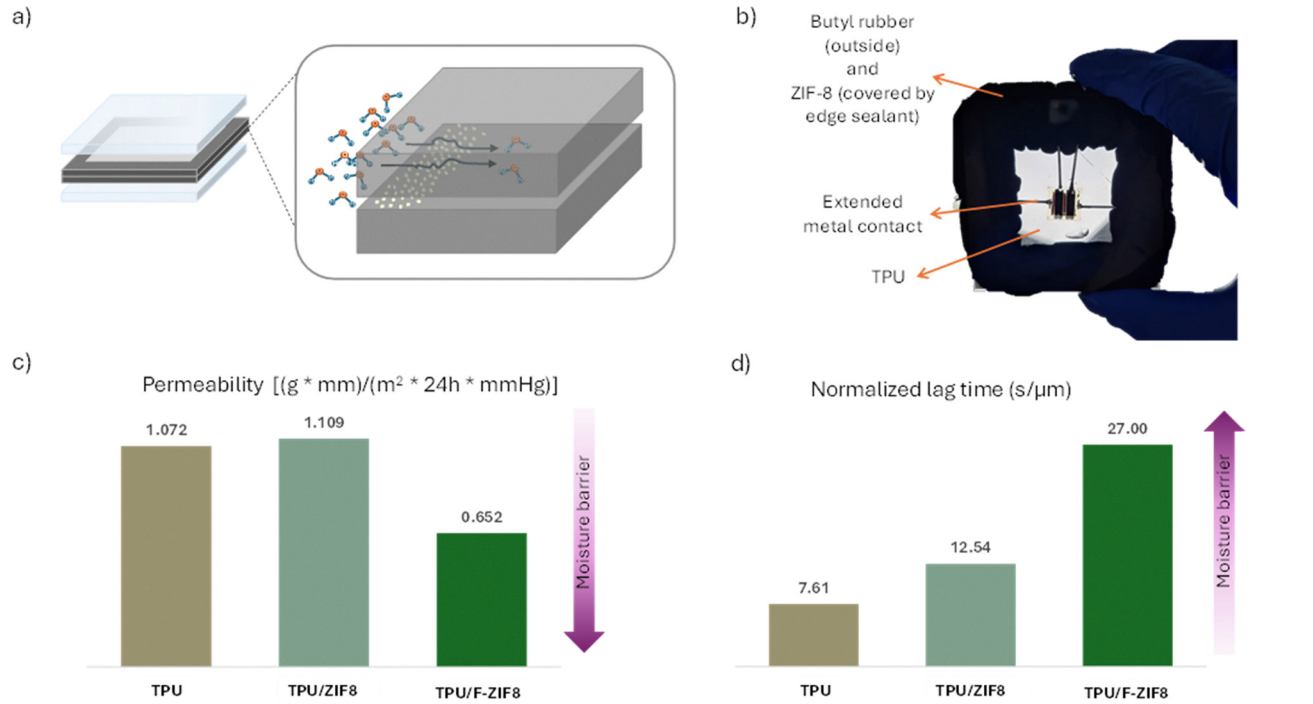

Fig. 2 Schematich illustration of the tortuous pathways mechanism that hinders transverse water molecule permeation (a); encapsulated device (b) permeability (c) and lag time (d) of reference samples, ZIF8, and modified F-ZIF8 measured at room temperature (RT) and 85% relative humidity (RH).

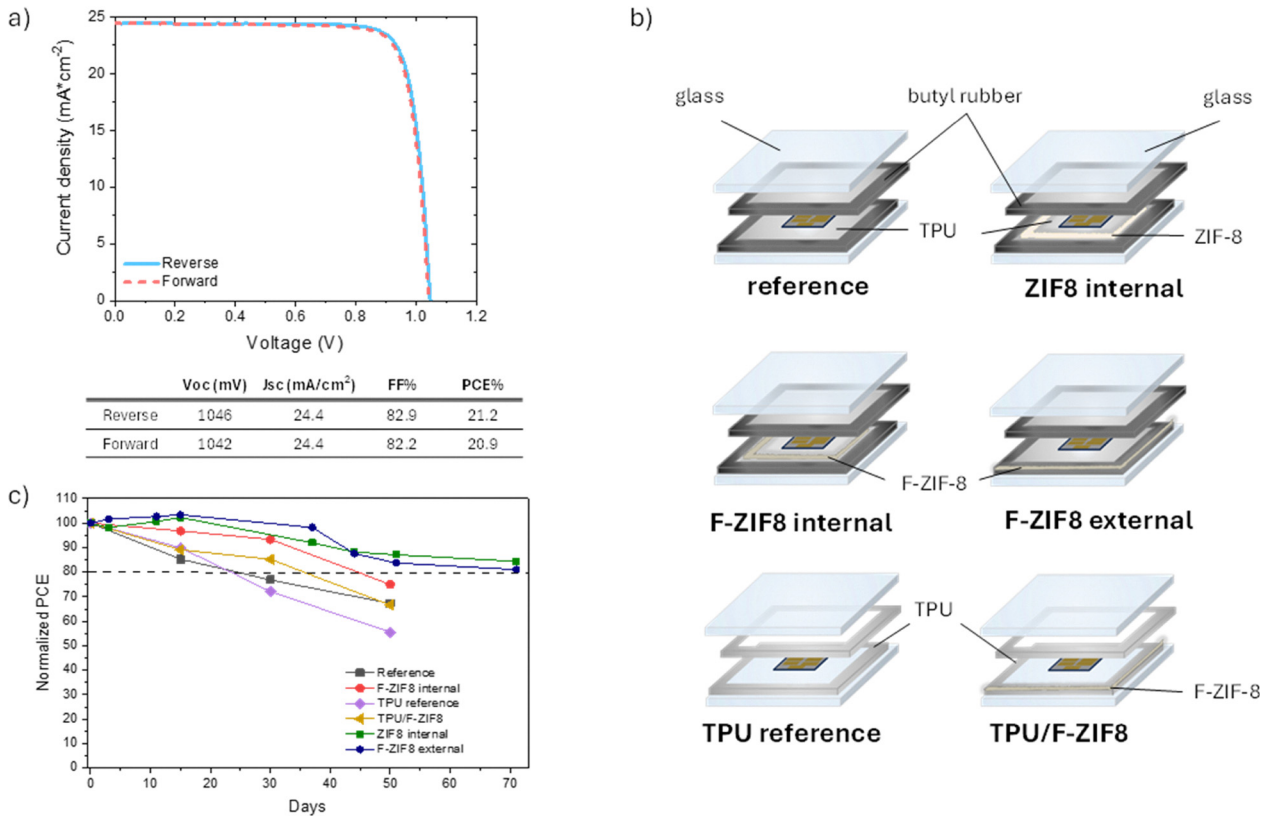

	Voc (mV)	Jsc (mA/cm²)	FF%	PCE%
Reverse	1046	24.4	82.9	21.2
Forward	1042	24.4	82.2	20.9

Fig. 3 *J*–*V* curve of reference sample after the encapsulation (a); schematic representation of the different layouts used (b); normalized efficiency of encapsulated PSCs over time under aging test conducted at 95%RH and RT (c).

in mixed matrix membranes (MMMs), lag time which is the delay before gas molecules begin permeating the polymer matrix is also critical, with higher lag times indicating improved encapsulation. As shown in Fig. 2(c), the permeability of TPU, measured under standard conditions of 23 °C and 85% RH, remains comparable to that of TPU/ZIF8, whereas TPU/F-ZIF8 exhibits a notable reduction in permeability. This improvement can be attributed to the super-hydrophobic nature of the fluorinated filler. Additionally, as seen in Fig. 2(d), the lag time normalized over the film thickness demonstrates an enhancement in barrier properties for the functionalized materials, increasing from 7 s μm^{-1} for unmodified TPU to 12 s μm^{-1} for TPU/ZIF8. The best results, however, were observed for TPU/F-ZIF8, which achieved a lag time of 27 s μm^{-1}, over three times that of the unmodified polymer. To explore the potential applications of the newly developed encapsulant, a set of $Cs_{0.03}MA_{0.07}FA_{0.9}PbI_3$ perovskite solar cells was encapsulated using various configurations, as shown in Fig. 3(b). The reference setup follows the standard glass–glass configuration commonly used for PSCs, with butyl rubber as the edge sealant and TPU as the internal cap sealant. For both sides, a layer of edge sealant and TPU was applied. The encapsulation process was carried out with an industrial laminator at 110 °C. The configurations labeled ZIF8 internal and F-ZIF8 internal were prepared with the same setup as the reference, with the specified filler added to the inner interface between the two TPU films prior to lamination. Another configuration, F-ZIF8 external, was prepared by drop-casting the filler solution onto the external surface of the edge sealant after lamination, followed by a brief 60 °C oven treatment to remove residual solvent. Additionally, a TPU-reference configuration was tested to evaluate the feasibility of replacing the butyl rubber edge sealant with TPU alone, without an internal cap sealant. In this configuration, modified F-ZIF8 was also applied to the external surface of the TPU edge sealant to examine its effectiveness. The aging test results at RT and 95% RH are presented in Fig. 3(c), where the normalized PCE over time demonstrates a clear trend. A key metric for evaluating PSC longevity is T_{80}, the time at which the cell retains 80% of its initial PCE after an aging test. If the normalized efficiency remains above T_{80}, the cell is considered operational. For the reference sample, T_{80} was reached 25 days. By contrast, both the ZIF8 internal and F-ZIF8 external samples showed significant improvements, with T_{80} extending beyond 70 days. Specifically, the ZIF8 internal sample retained 84% of its initial PCE after 70 days, while the modified ZIF8 external sample retained 81% after the same period. The F-ZIF8 internal configuration reached T_{80} at 45 days, indicating an enhanced lifespan compared to the reference, though with lower stability compared to other layouts. This suggests that the modified ZIF-8, containing an apolar fluorinated group, may not be fully compatible with the polar carbamate groups in TPU, potentially causing segregation at the filler/polymer interface and the formation of defects in the MMM that could reduce the barrier performance. This issue was not observed with the modified ZIF-8 external configuration, as the filler was applied on the outer surface of the edge sealant. The TPU-reference sample, as expected, exhibited lower encapsulation performance, with T_{80} similar to the reference sample using butyl rubber as the edge sealant but showing faster degradation overall. The TPU/F-ZIF8 external configuration demonstrated improved encapsulation performance, achieving a T_{80} of 35 days, underscoring the potential of F-ZIF8 applied on the outer surface to enhance barrier properties.

Conclusion

In this work, we enhanced the barrier performance of commercial TPU ST-6050 by incorporating ZIF8 into a mixed-matrix membrane (MMM), exploiting the resulting tortuous-pathway effect. Permeability measurements, including lag-time analysis, revealed that ZIF8 functionalization markedly increases moisture resistance, with the fluorinated-silane-modified F-ZIF8 variant delivering a lag time three times greater than unmodified TPU. Contact-angle assays confirmed a corresponding boost in surface hydrophobicity. To assess encapsulation performance under stress, p–i–n $Cs_{0.03}MA_{0.07}FA_{0.9}PbI_3$ cells were sealed with TPU/ZIF8 MMMs and aged at 25 °C, 95% RH. Devices with unmodified ZIF8 in the interlayer retained 84% of their initial PCE ($T_{80} > 70$ days), while those using the fluorinated F-ZIF8 on the outer interface retained 81% after the same period. These results demonstrate that ZIF8-reinforced TPU provides a low-temperature, high-performance encapsulant suitable for PSCs with limited thermal tolerance where POE is impractical paving the way for a new encapsulation strategy which can be adopted on larger area.

Conflicts of interest

There are no conflicts to declare.

Data availability

All data including software, datasets, data presented in an article (*e.g.*, in figures or tables) are available upon request to the first author or the corresponding author.

Supplementary information (SI) is available. See DOI: **https://doi.org/10.1039/d5tc03451e**.

Acknowledgements

The authors also thankful to The Ministero dell'Università e della Ricerca (MUR), University of Pavia, through the program ''Dipartimentidi Eccellenza 2023–2027'' for fundings. F. T. and G. G. acknowledge the support of HERO Project through King Abdullah University of Science and 607 Technology (KAUST). L. P. F. F. thanks the PhD fellowship co-founded by the European Union – FSE, Programma Operativo Nazionale (PON) Ricerca e Innovazione 2014–2020 (CCI 2014IT16M2OP005). G. G. acknowledges the SPIKE project, which received funding from a European Research Council Proof of Concept 2022 grant under the

European Union's Horizon 2020 research and innovation programme (grant agreement number 101068936).

Notes and references

1 B. P. Kore, M. Jamshidi and J. M. Gardner, *Mater. Adv.*, 2024, **5**, 2200–2217.
2 J. Wei, Q. Wang, J. Huo, F. Gao, Z. Gan, Q. Zhao and H. Li, *Adv. Energy Mater.*, 2021, **11**, 2002326.
3 H. Shahivandi, M. Vaezzadeh and M. Saeidi, *Sol. Energy Mater. Sol. Cells*, 2020, **208**, 110383.
4 C. C. Boyd, R. Cheacharoen, T. Leijtens and M. D. McGehee, *Chem. Rev.*, 2019, **119**, 3418–3451.
5 J. Li, R. Xia, W. Qi, X. Zhou, J. Cheng, Y. Chen, G. Hou, Y. Ding, Y. Li, Y. Zhao and X. Zhang, *J. Power Sources*, 2021, **485**, 229313.
6 A. Uddin, M. B. Upama, H. Yi and L. Duan, *Coatings*, 2019, **9**, 65.
7 Y. Wang, I. Ahmad, T. Leung, J. Lin, W. Chen, F. Liu, A. M. C. Ng, Y. Zhang and A. B. Djurišić, *ACS Mater. Au*, 2022, **2**, 215–236.
8 F. Corsini and G. Griffini, *J. Phys. Energy*, 2020, **2**, 031002.
9 L. Xiang, F. Gao, Y. Cao, D. Li, Q. Liu, H. Liu and S. Li, *Org. Electron.*, 2022, **106**, 106515.
10 Y. H. Soo, S. A. Ng, Y. H. Wong and C. Y. Ng, *J. Mater. Sci.: Mater. Electron.*, 2021, **32**, 14885–14900.
11 D. a I. Jiaqi, Z. Dong and W. U. Xiaoshan, *Prog. Phys.*, 2024, **44**, 19.
12 E. Young Choi, J.-H. Kim, B.-J. Kim, J. Hun Jang, J. Kim and N. Park, *RSC Adv.*, 2019, **9**, 11737–11744.
13 Y. I. Lee, N. J. Jeon, B. J. Kim, H. Shim, T.-Y. Yang, S. I. Seok, J. Seo and S. G. Im, *Adv. Energy Mater.*, 2018, **8**, 1701928.
14 J. Idígoras, F. J. Aparicio, L. Contreras-Bernal, S. Ramos-Terrón, M. Alcaire, J. R. Sánchez-Valencia, A. Borras, Á. Barranco and J. A. Anta, *ACS Appl. Mater. Interfaces*, 2018, **10**, 11587–11594.
15 N. Kr Rana, S. Debata, S. Kr Panda, D. Pratap Singh and N. Chander, *Sol. Energy*, 2024, **280**, 112874.
16 Z. Zheng, Z. Xue, K. Zhao, Y. Yang, X. Zhu, H. Li, S. Cheng, S. Li, N. Yan and Z. Wang, *Sol. RRL*, 2024, **8**, 2301076.
17 H. Wang, Y. Zhao, Z. Wang, Y. Liu, Z. Zhao, G. Xu, T.-H. Han, J.-W. Lee, C. Chen, D. Bao, Y. Huang, Y. Duan and Y. Yang, *Nano Energy*, 2020, **69**, 104375.
18 R. Cheacharoen, C. C. Boyd, G. F. Burkhard, T. Leijtens, J. A. Raiford, K. A. Bush, S. F. Bent and M. D. McGehee, *Sustainable Energy Fuels*, 2018, **2**, 2398–2406.
19 L. Mu, S. Wang, H. Liu, W. Li, L. Zhu, H. Wang and H. Chen, *Adv. Funct. Mater.*, 2025, **35**, 2415353.
20 P. Holzhey and M. Saliba, *J. Mater. Chem. A*, 2018, **6**, 21794–21808.
21 X. Li, M. Tschumi, H. Han, S. S. Babkair, R. A. Alzubaydi, A. A. Ansari, S. S. Habib, M. K. Nazeeruddin, S. M. Zakeeruddin and M. Grätzel, *Energy Technol.*, 2015, **3**, 551–555.
22 M. D. Kempe, G. J. Jorgensen, K. M. Terwilliger, T. J. McMahon, C. E. Kennedy and T. T. Borek, *Sol. Energy Mater. Sol. Cells*, 2007, **91**, 315–329.
23 R. Cheacharoen, N. Rolston, D. Harwood, K. A. Bush, R. H. Dauskardt and M. D. McGehee, *Energy Environ. Sci.*, 2018, **11**, 144–150.
24 S. Ma, G. Yuan, Y. Zhang, N. Yang, Y. Li and Q. Chen, *Energy Environ. Sci.*, 2022, **15**, 13–55.
25 "Designing New Materials for Photovoltaics: Opportunities for Lowering Cost and Increasing Performance through Advanced Material Innovations," ISBN 978-3-907281-02-4, Report IEAPVPS T13-13:2021, April 2021.
26 Thermomechanical fatigue of solder joint and interconnect ribbon: impact of low lamination temperature, DOI: 10.4229/EUPVSEC20212021-4BO.5.4.
27 L. La Notte, G. Polino, P. Verzola, L. Salamandra, F. Brunetti, T. M. Brown, A. Di Carlo and A. Reale, *Surf. Coat. Technol.*, 2014, **255**, 69–73.
28 R. K. Raman, S. Ganesan, A. Alagumalai, V. Sudhakaran Menon, S. A. Gurusamy Thangavelu and A. Krishnamoorthy, *ACS Appl. Mater. Interfaces*, 2023, **15**, 53935–53950.
29 M. Benzaqui, R. Semino, N. Menguy, F. Carn, T. Kundu, J.-M. Guigner, N. B. McKeown, K. J. Msayib, M. Carta, R. Malpass-Evans, C. Le Guillouzer, G. Clet, N. A. Ramsahye, C. Serre, G. Maurin and N. Steunou, *ACS Appl. Mater. Interfaces*, 2016, **8**, 27311–27321.
30 W. Miao, J. Wang, J. Liu and Y. Zhang, *Adv. Mater. Interfaces*, 2018, **5**, 1800167.
31 Y. Yue, Y. Zhang, Y. Zheng, Y. Shao, B. Wei and W. Shi, *Energy Technol.*, 2025, **13**, 2402310.
32 Z. Skafi, L. A. Castriotta, B. Taheri, F. Matteocci, M. Fahland, F. Jafarzadeh, E. Joseph, A. Chakraborty, V. Singh, V. Mottaghitalab, L. Mivehi, F. Brunetti, L. Sorbello, A. Di Carlo and T. M. Brown, *Adv. Energy Mater.*, 2024, **14**, 2400912.

